

## ARTICLE TYPE

# The cosmological Mass Varying Neutrino model in the late universe

Olga Avsajanishvili\*<sup>1</sup>

<sup>1</sup>Evgeni Kharadze Georgian National Astrophysical Observatory, 47/57 Kostava Str., Tbilisi 0179, Georgia

<sup>2</sup>School of Natural Sciences and Medicine, Ilia State University, 3/5 Cholokashvili Ave., Tbilisi 0162, Georgia

## Correspondence

\*Olga Avsajanishvili. Email: olga.avsajanishvili@iliauni.edu.ge

## Present Address

E.Kharadze Georgian National Astrophysical Observatory, 47/57 Kostava Str., Tbilisi 0179, Georgia

## Funding Information

Shota Rustaveli National Science Foundation of Georgia (SRNSFG), YS-22-998. Shota Rustaveli National Science Foundation of Georgia (SRNSFG), YS-22-998.

The cosmological Mass Varying Neutrino (MaVaN) model beyond the standard  $\Lambda$ CDM scenario is considered. The interaction of the fermionic field and the scalar field with the inverse power law Ratra-Peebles potential via the Yukawa coupling is studied in detail. Depending on the model parameter  $\alpha$  of the Ratra-Peebles potential of the scalar field, the expansion rate of the universe, the mass equation, the mass of the scalar field, the sum of neutrino masses, the mutual influence of the sum of neutrino masses and the value of the Ratra-Peebles potential of the scalar field, as well as the total density of the thermodynamic potential of the coupled fermionic and scalar fields at the critical point are explored. The observational constraints of the parameters of the flat and non-flat MaVaN models have been carried out from the 32  $H(z)$  data using the MCMC analysis. The parameters were obtained for the flat MaVaN model: Hubble constant  $H_0 = 64.04^{+1.48}_{-3.69}$  km s<sup>-1</sup>Mpc<sup>-1</sup>, the model parameter of the scalar field Ratra-Peebles potential  $\alpha = 0.008^{+0.003}_{-0.006}$ , the matter density parameter in the present epoch  $\Omega_{m0} = 0.341^{+0.056}_{-0.050}$ , the sum of neutrino masses  $m_\nu \leq 0.396$  eV (1 $\sigma$  confidence level); while for the non-flat MaVaN model:  $H_0 = 67.72^{+3.50}_{-6.47}$  km s<sup>-1</sup>Mpc<sup>-1</sup>,  $\alpha = 0.01^{+0.004}_{-0.009}$ ,  $\Omega_{m0} = 0.396^{+0.079}_{-0.046}$ ,  $m_\nu \leq 0.473$  eV (1 $\sigma$  confidence level), the curvature density parameter in the present epoch  $\Omega_{k0} = -0.214^{+0.176}_{-0.187}$ . We conclude that the  $H_0$  tension is resolved in the flat MaVaN model within the 3 $\sigma$  confidence level and in the non-flat MaVaN model within the 2 $\sigma$  one.

## KEYWORDS:

cosmology, dark energy, scalar field, neutrinos mass, Bayesian statistics

## 1 | INTRODUCTION

The standard spatially flat  $\Lambda$ CDM cosmological model (Caldwell & Kamionkowski, 2009; Peebles, 1984; Peebles & Ratra, 2003; Silvestri & Trodden, 2009) (for a recent review, see (Lopez-Corredoira, 2023)) agrees well with various observational constraints obtained over the past decades (Aghanim & et al., 2020a, 2020b; Aiola & et al., 2020; Alam & et al., 2021).

Being still a fiducial cosmological model at present, the  $\Lambda$ CDM model has several, statistically significant tensions

and anomalies with various datasets, the number of which increases as more accurate observational data are obtained (for recent comprehensive reviews, see (Abdalla & et al., 2022; Di Valentino, 2022; Di Valentino et al., 2021; Hu & Wang, 2023; Moresco & et al., 2022; Peebles, 2022; Perivolaropoulos & Skara, 2022; Vagnozzi, 2023)).

Among these discrepancies, one of the most prominent is the tension on the Hubble constant  $H_0$ , which manifests itself as a discrepancy of more than 5 $\sigma$  in the measured value of  $H_0$  when comparing Planck Cosmic Microwave Background data Aghanim and et al. (2020b) with local distance ladder estimates, namely the SH0ES collaboration (Riess et al., 2022).

The presence of still unsolved problems in the  $\Lambda$ CDM model inspires and stimulates cosmologists to explore dark energy models that go beyond the  $\Lambda$ CDM model (Abdalla & et al., 2022; Di Valentino et al., 2021; Khalife et al., 2024). The dynamical scalar field  $\phi$ CDM models are one of many alternatives to the  $\Lambda$ CDM model. In these models, dark energy is represented in the form of a uniform cosmological scalar field that slowly varies in the present epoch (Ratra & Peebles, 1988a, 1988b; Wetterich, 1988). In these models, the energy density and pressure are time dependent functions under the assumption that the scalar field is described by the ideal barotropic fluid model.

One of the unresolved issues in modern cosmology is the coincidence problem (Comelli, Pietroni, & Riotto, 2003; Kawasaki, Murayama, & Yanagida, 1992; Velten, vom Marttens, & Zimdahl, 2014), the essence of which is that at the present epoch, the density of dark energy is comparable to the energy density of dark matter, despite the fact that in the past they changed differently over time. Based on this, it can be assumed that dark matter and dark energy could somehow interact with each other in the course of their evolution. Various interacting dark energy models have been proposed to provide a possible solution to the coincidence problem in the  $\Lambda$ CDM model (Berger & Shojaei, 2006; Cai & Wang, 2005; del Campo, Herrera, & Pavon, 2008, 2009; Fardon, Nelson, & Weiner, 2004; Farrar & Peebles, 2004; Huey & Wandelt, 2006; Pavon & Zimdahl, 2005).

In its turn, dark matter is comparable, in order of magnitude, to the energy density of neutrinos (Dolgov, 2008; Hannestad, 2004; Ivanchik, Kurichin, & Yurchenko, 2024). Various experiments confirmed that neutrinos have mass (Tanabashi & et al., 2018), but the origin of neutrinos mass is still an unresolved issue. Stringent constraints on the sum of neutrino masses were obtained by different state-of-the-art cosmological measurements (Abdul Karim & et al., 2025; Adame & et al., 2024, 2025; Aghanim & et al., 2020a, 2020b; Alam & et al., 2021; Elbers & et al., 2025; Jiang et al., 2025; Madhavacheril & et al., 2024; Naredo-Tuero, Escudero, Fernández-Martínez, Marcano, & Poulin, 2024; Palanque-Delabrouille et al., 2020; Tristram & et al., 2024). The latest cosmological constraint on the upper limits on the sum of neutrino masses  $m_\nu(a_0) < 0.0642$  eV was established through measurements of baryon acoustic oscillations (BAO) from Data Release 2 (DR2) by the Dark Energy Spectroscopic Instrument (DESI) (Elbers & et al., 2025) in galaxies and Lyman- $\alpha$  forest tracers. However, the Karlsruhe Tritium Neutrino Experiment (KATRIN), which directly measured the neutrinos mass, has reported an upper limit  $m_\nu(a_0) < 0.45$  eV Aker and et al. (2025).

Fardon, Nelson and Weiner elaborated the mechanism of Varying Mass Particles (VAMPs) (Fardon et al., 2004). They

applied this mechanism in the context of neutrinos, as a result of which the Mass Varying Neutrino (MaVaN) model was created. In this model, the neutrinos, *i.e.*, fermionic field interacts with the scalar field via the Yukawa coupling. If the decoupled neutrino field is initially massless, then the coupling generates a mass of neutrinos, which subsequently changes over time (Farrar & Peebles, 2004). The MaVaN scenario is quite compelling, since it connects the origin of neutrino masses to dark energy, and solves the coincidence problem of the  $\Lambda$ CDM model. However, there are some problems that need to be addressed for the MaVaN scenario to be viable (Afshordi, Zaldarriaga, & Kohri, 2005; Bean, Flanagan, & Trodden, 2008a, 2008b; Bjaelde et al., 2008; Brookfield, van de Bruck, Mota, & Tocchini-Valentini, 2006b; Ichiki & Keum, 2008; Kaplinghat & Rajaraman, 2007). One of these is related to the strong instability in the MaVaN model due to the negative square of the sound speed of the neutrinos-scalar field fluid (Afshordi et al., 2005; Bean et al., 2008a, 2008b). The coupling between neutrinos almost stops the evolution of the scalar field and triggers an accelerated expansion of the universe (Collodel & Kremer, 2012; Wetterich, 2007). The exponential clustering of the neutrino occurs due to the exponential growth of scalar perturbations in the MaVaN model (Afshordi et al., 2005; Ayaita, Weber, & Wetterich, 2013; Casas, Pettorino, & Wetterich, 2016; Kaplinghat & Rajaraman, 2007; Mota, Pettorino, Robbers, & Wetterich, 2008; Nunes, Schrempp, & Wetterich, 2011; Pettorino & Baccigalupi, 2008; Pettorino, Wintergerst, Amendola, & Wetterich, 2010). The effect of the neutrinos-scalar field fluid in the MaVaN model on various cosmological observations has been studied in many papers, including (Brookfield, van de Bruck, Mota, & Tocchini-Valentini, 2006a; Brouzakis, Pettorino, Tetradis, & Wetterich, 2011; Goh, Ocampo, Nesseris, & Pettorino, 2024; Pettorino et al., 2010).

Within the MaVaN model, Chitov, August, Natarajan, and Kahniashvili (2011) analyzed the thermal evolution of the universe and predicted its stable, metastable, and unstable phases. They found that the universe in the present epoch is below its critical temperature, and the state of the universe is similar to a supercooled liquid that has not yet crystallized: its high-temperature (meta)stable phase has become unstable, but the new low-temperature stable phase has not yet been reached.

Mandal, Chitov, Avsajanishvili, Singha, and Kahniashvili (2021) found that depending on the choice of the scalar field potential, the acceleration of the universe occurs in an instability regime or in a stable regime in the MaVaN model.

Mandal and Sehgal (2023) considered the interaction of the fermionic field and the scalar field with the exponential potential in the MaVaN model. They found that the current relic dark matter density is reached at fermion masses in the range of  $1 \text{ GeV} - 10^9 \text{ GeV}$  for the phase transition (after which the coupled neutrinos-scalar field fluid behaves as pressureless dark matter) temperature range of  $10 \text{ MeV} - 10^7 \text{ GeV}$ .

In the framework of the MaVaN model, we explored in detail the interaction of the fermionic field and the scalar field with the inverse power law Ratra-Peebles potential in the late epoch of the universe. In studying the MaVaN model, we used the formalism and approach elaborated in (Chitov et al. (2011)), but unlike the study of (Chitov et al. (2011)), which considered a number of neutrinos flavors  $N_F = 1$ , we performed calculations for  $N_F = 3$ .

This paper is organized as follows: the main equations for the MaVaN model are presented in Section 2, the interaction of the fermionic field and the scalar field with the Ratra-Peebles potential is considered in Section 3, observational constraints of the parameters flat and non-flat MaVaN models are described in Section 4, the results of the calculations are represented in Section 5, and the conclusions are summarized in Section 6. We used the natural system of units,  $c = k_B = 1$ .

## 2 | THE GENERAL DESCRIPTION OF THE MAVAN MODEL

We assumed that the flat, homogeneous and isotropic universe is described by the Friedmann-Lemaître-Robertson-Walker spacetime metric,  $ds^2 = dt^2 - a^2(t)d\mathbf{x}^2$ , here  $t$  is a cosmic time,  $a(t)$ <sup>1</sup> is a scale factor (normalized to be unity in the present epoch  $a_0 \equiv a(t_0)$ ),  $\mathbf{x}$  are the comoving coordinates.

The Euclidean action of the scalar field is defined as

$$S_B^E = \int_0^\beta d\tau \int a^3 d^3x \left[ \frac{1}{2} \left( \frac{\partial \phi}{\partial \tau} \right)^2 + \frac{(\nabla \phi)^2}{2a^2} + V(\phi) \right], \quad (1)$$

here  $\tau = it$ ,  $\int d^3x = V_{com}$  is a comoving volume;  $a^3 \int d^3x = V_{phys}$  is a physical volume;  $V(\phi)$  is a potential of the scalar field.

The Euclidean action for the Dirac field has a form

$$S_D^E = \int_0^\beta d\tau \int a^3 d^3x \bar{\psi}(\mathbf{x}, \tau) \hat{D}(\phi) \psi(\mathbf{x}, \tau), \quad (2)$$

here  $\hat{D}(\phi) = \gamma^\circ \frac{\partial}{\partial \tau} - \frac{i\gamma}{a} \cdot \nabla + g\phi(\mathbf{x}, \tau) - \mu\gamma^\circ$  is the Dirac operator.

The pressure  $P_D$  is defined as

$$P_D = -P_0 + \frac{1}{3\pi^2} \int_0^\infty \frac{k^4 dk}{\epsilon(k)} \left[ n_F(\epsilon_-) + n_F(\epsilon_+) \right], \quad (3)$$

here  $P_0 = 2 \int k d^3\epsilon(k)/(2\pi)^3$  is the vacuum contribution to the pressure;  $\epsilon(k) = \sqrt{k^2 + m_v^2}$ ,  $\epsilon_\pm = \epsilon \pm \mu$ ,  $\mu$  is the chemical potential<sup>2</sup>,  $k$  is the Fermi momentum,  $m_v$  is the fermionic mass;  $n_F(x) \equiv (e^{\beta x} + 1)^{-1}$  is the Fermi distribution function,  $\beta = 1/T_v$  is the inverse temperature  $T_v$ ,  $T_v = T_{v0}/a$  is the temperature of the fermions at the scale factor  $a$  and  $T_{v0} = 1.9454 \text{ K} = 2.35 \cdot 10^{-4} \text{ eV}$  is the temperature of the fermions in the present epoch.

The interaction of the bosonic scalar field with the massless fermions via the Yukawa coupling described by the action

$$S_{BD}^E = S_B^E + S_D^E = \left|_{m_v=0} \right. + g \int_0^\beta d\tau \int a^3 d^3x \phi \bar{\psi} \psi, \quad (4)$$

where  $g$  is the Yukawa coupling constant<sup>3</sup>.

The fermionic mass is generated due to the violation of chiral symmetry in the Dirac sector of the Lagrangian Eq. (4), the value of the fermionic mass subsequently changes over time. The path integral for the partition function in the interaction of the scalar field with the fermionic field is

$$\mathcal{Z} = \int D\phi D\bar{\psi} D\psi e^{-S_{BD}^E}. \quad (5)$$

The Grassmann fields can be formally integrated (Kapusta & Gale, 2011) as

$$\mathcal{Z} = \int D\phi e^{-S_{BD}^E} = \int D\phi \exp(-S_{BD}^E + \log \text{Det } \hat{D}(\phi)). \quad (6)$$

The total thermodynamic potential of the coupled fermionic and scalar fields is

$$V_{\phi v} = V(\phi) + V_v(\phi) = V(\phi) - \frac{2N_F}{3\pi^2\beta^4} \int_{\frac{\phi}{\bar{\phi}}}^\infty \frac{(x^2 - \bar{\phi}^2)^{3/2}}{e^x + 1} dx, \quad (7)$$

here  $N_F$  is a number of neutrinos flavors, which we considered  $N_F = 3$  in our calculations; the dimensionless variable  $\bar{\phi} = g\beta\phi$  (Chitov et al., 2011).

The total thermodynamic potential of the coupled fermionic and scalar fields can be found in the saddle-point approximation, minimizing the path integral, Eq. (6). The saddle-point approximation coincides with the minimum condition of the total thermodynamic potential at equilibrium for the fixed temperature and the chemical potential values at the critical point  $a_{cr}$

$$\left. \frac{\partial V_{\phi v}}{\partial \phi} \right|_{v, \beta, \phi = \phi_{cr}} = 0, \quad \left. \frac{\partial^2 V_{\phi v}}{\partial \phi^2} \right|_{v, \beta, \phi = \phi_{cr}} > 0. \quad (8)$$

<sup>1</sup>Below, for simplicity of notation, we omit the explicit dependence of the scalar factor on time, while implying the dependence of the scalar factor on time.

<sup>2</sup>In the simplified model, considered in (Chitov et al., 2011) and here,  $\mu = 0$ .

<sup>3</sup>As well as in (Chitov et al., 2011), we set the value  $g = 1$  in our calculations.

As a consequence, neutrinos acquire mass at the critical point

$$a_{cr} \quad \left. \frac{\partial V_{\phi\nu}}{\partial \phi} \right|_{\phi=\phi_{cr}} = \left. \frac{\partial V(\phi)}{\partial \phi} \right|_{\phi=\phi_{cr}} + \left. \frac{\partial V_\nu(\phi)}{\partial \phi} \right|_{\phi=\phi_{cr}}, \quad (9)$$

here  $\phi(a_{cr}) = \phi_{cr}$  is the average of the bosonic field,  $\phi_{cr} = \langle \phi \rangle$ , and the fermionic mass is defined as  $m_\nu = g\phi_{cr}$  (Chitov et al. (2011)).

The Eq. (9) can be represented as

$$V'(\phi) \Big|_{\phi=\phi_{cr}} + g\rho_s = 0, \quad (10)$$

where  $\rho_s$  is the scalar fermionic density (or the chiral density) that is given by

$$\rho_s = \frac{m_\nu}{\pi^2} \int_0^\infty \frac{dk k^2}{\epsilon(k)} \left[ n_F(\epsilon_+) + n_F(\epsilon_-) - 1 \right]. \quad (11)$$

### 3 | INTERACTION OF THE FERMIONIC FIELD AND THE SCALAR FIELD WITH THE RATRA-PEEBLES POTENTIAL

#### 3.1 | Scalar field with the Ratra-Peebles potential. Mass equation

We studied the interaction of the fermionic field and the scalar field with the inverse power law Ratra-Peebles potential (Ratra & Peebles, 1988a, 1988b), which has a form

$$V(\phi) = \frac{M^{\alpha+4}}{\phi^\alpha}, \quad (12)$$

here  $M$  and  $\alpha$  are positive model parameters. The parameter  $M$  is the scale mass of the Ratra-Peebles potential; the parameter  $\alpha$  defines the steepness of the potential, for  $\alpha = 0$ , the scalar field  $\phi$ CDM model reduces to the standard  $\Lambda$ CDM model. A three-dimensional representation of the Ratra-Peebles potential is shown in Fig. 1

The total thermodynamic potential of the coupled fermionic and scalar fields with the Ratra-Peebles potential at the critical point  $a_{cr}$  reads as follows

$$V_{\phi\nu} = \frac{M^{\alpha+4}}{\phi^\alpha} - \frac{2N_F}{3\pi^2\beta^4} \int_{\bar{\phi}}^\infty \frac{(x^2 - \bar{\phi}^2)^{3/2}}{e^x + 1} dx. \quad (13)$$

The dimensionless density of the total thermodynamic potential of the coupled fermionic and scalar fields with the Ratra-Peebles potential can be obtained from Eq. (13) as

$$\bar{V}_{\phi\nu} = \frac{V_{\phi\nu}}{M^4} = \left( \frac{\bar{M}}{\bar{\phi}} \right) - \frac{2N_F}{3\pi^2\bar{M}^4} \int_{\bar{\phi}}^\infty \frac{(x^2 - \bar{\phi}^2)^{3/2}}{e^x + 1} dx, \quad (14)$$

$\bar{M} = \beta M$  and  $\bar{\phi} = g\beta\phi$  are dimensionless variables (Chitov et al., 2011).

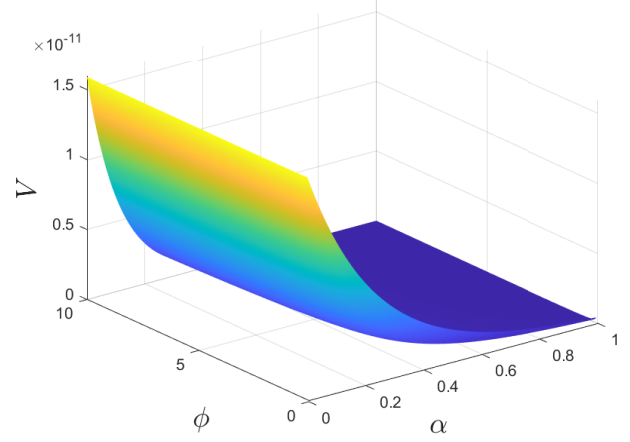


**FIGURE 1** A three-dimensional representation of the Ratra-Peebles potential for  $M = 2 \cdot 10^{-3}$  eV

The mass equation  $I_\alpha(\bar{\phi})$  was derived by finding the minimum condition of the total thermodynamic potential, Eq. (14) at the critical point  $a_{cr}$

$$\frac{\alpha\pi^2 g^\alpha \bar{M}^{\alpha+4}}{2N_F} = I_\alpha(\bar{\phi}), \quad (15)$$

where

$$I_\alpha(\bar{\phi}) = \bar{\phi}^{\alpha+2} \int_{\bar{\phi}}^\infty \frac{(x^2 - \bar{\phi}^2)^{1/2}}{e^x + 1} dx. \quad (16)$$

#### 3.2 | Basic equations describing the neutrinos-scalar field fluid

Before interaction with the scalar field, neutrinos are in the free-streaming regime, being massless and relativistic. After the critical point, neutrinos become non-relativistic, *i.e.*, the chiral density of neutrinos scales as  $\rho_\nu \propto a^{-3}$  for  $a \geq a_{cr}$ . During this period of time, the formation of the neutrinos-scalar field fluid occurs.

The neutrinos-scalar field fluid is characterized by the total effective potential consisting of the Ratra-Peebles potential and the additional component connected to neutrinos

$$V_{couple} = \frac{M^{\alpha+4}}{\phi^\alpha} + \phi \rho_{cr} \left( \frac{a_{cr}}{a} \right)^3, \quad (17)$$

here  $\rho_{cr} = \alpha(\Delta_{cr}/\nu)^{(\alpha+1)} M^3$  is a value of the chiral density at the critical point;  $\Delta_{cr} = \left( \frac{\sqrt{2}\nu e^{-\nu}}{\alpha\pi^{3/2}} \right)^{-(\alpha+4)}$ , with  $\nu = \alpha + 5/2$ ,  $M = (\nu^\alpha \rho_{\phi\nu 0})^{(\alpha+1)/(\alpha+4)} \Delta_{cr}^{-\alpha} T_{\nu 0}^{-3\alpha/(\alpha+4)}$  (Chitov et al., 2011);  $\rho_{\phi\nu 0} \approx 2.76 \cdot 10^{-11} h^2 \text{ eV}^4$  is the density of the

neutrinos-scalar field fluid in the present epoch, with  $h = 0.674$  (Aghanim & et al., 2020b).

The first Friedmann equation and the scalar field Klein-Gordon equation of motion of the neutrinos-scalar field fluid are respectively read as

$$E = \left( \Omega_{m0} a^{-3} + \Omega_{k0} a^{-2} + \frac{1}{\rho_{cr0}} \left( \frac{\dot{\phi}^2}{2} + \frac{M^{\alpha+4}}{\phi^\alpha} + \phi \rho_{cr} \left( \frac{a_{cr}}{a} \right)^3 \right) \right)^{1/2} \quad (18)$$

$$\ddot{\phi} + 3\dot{\phi} - \frac{\alpha M^{\alpha+4}}{\phi^{\alpha+1}} + \rho_{cr} \left( \frac{a_{cr}}{a} \right)^3 = 0, \quad (19)$$

here  $E = H/H_0$  is the normalized Hubble parameter,  $H$  is the Hubble parameter,  $H_0$  the value of the Hubble parameter in the present epoch,  $H_0 = 100 \cdot h \text{ km s}^{-1} \text{ Mpc}^{-1}$ ;  $\Omega_{m0}$  and  $\Omega_{k0}$  are the matter and curvature density parameters in the present epoch,  $\Omega_{m0} = 0.315$  Aghanim and et al. (2020b);  $\rho_{cr0} \approx 4.31 \cdot 10^{-11} h^2 \text{ eV}^4$  is the critical energy density in the present epoch.

The mass of the scalar field with the Ratra-Peebles potential is defined as

$$m_\phi = \left( \frac{\partial^2 V}{\partial \phi^2} \right)^{1/2} \Big|_{\phi=\phi_{cr}} = \left( \alpha(\alpha+1) M^{\alpha+4} \phi^{-(\alpha+2)} \right)^{1/2}. \quad (20)$$

## 4 | OBSERVATIONAL CONSTRAINTS OF THE PARAMETERS FLAT AND NON-FLAT MAVAN MODELS

To constrain the parameters  $\mathbf{p} = \{H_0, \alpha, \Omega_{m0}, m_\nu\}$  and  $\mathbf{p} = \{H_0, \alpha, \Omega_{m0}, m_\nu, \Omega_{k0}\}$  of the flat and non-flat MaVaN models, respectively, we used 32  $H(z)$  measurements in the redshift range of  $0.07 \leq z \leq 1.965$  presented in (Cao & Ratra, 2023). Of which 15 measurements are correlated (Moresco, 2015; Moresco et al., 2012; Moresco et al., 2016). The covariance matrix for these correlated measurements can be found at <https://gitlab.com/mmoresco/CCcovariance/>.

In our analysis, we used the following priors for the parameters<sup>4</sup>.

**TABLE 1** Priors for the parameters in the MaVaN model.

Parameter	Priors
$H_0$	[None, None]
$\alpha$	[0.0001, 0.04]
$\Omega_{m0}$	[0.15, 0.6]
$m_\nu$	[0.0001, 0.6]
$\Omega_{k0}$	[-0.6, 0.6]

We sampled the posterior distributions of the MaVaN model parameters using Markov Chain Monte Carlo (MCMC) method via the Cobaya framework (Torrado & Lewis, 2021). In addition, we applied the PYTHON GETDIST package (Lewis, 2019) to create plots and analyze the MCMC results. Chain convergence was rigorously validated using the Gelman-Rubin diagnostic, achieving  $R-1 = 0.022636$  and  $R-1 = 0.036264$ , for flat and non-flat MaVaN models, respectively, which satisfies the conventional threshold of  $R-1 \leq 0.1$  (Gelman & Rubin, 1992) and indicates robust sampling of the target distribution. The best-fit model was selected by minimizing the  $\chi^2$  statistic, calculated from the discrepancy between theoretical predictions and observational  $H(z)$  data. Our analysis yielded  $\chi_{min}^2 = 15.32$  and  $\chi_{min}^2 = 15.01$  for flat and non-flat MaVaN models, respectively. The corresponding reduced values of  $\chi_{min}^2$ ,  $\chi_{red}^2 = 0.5471$  and  $\chi_{red}^2 = 0.5559$ , for flat and non-flat MaVaN models, respectively, demonstrate reasonable consistency between the MaVaN model and constraints by the  $H(z)$  data, without statistically significant tension.

## 5 | RESULTS AND DISCUSSIONS

### 5.1 | Studying features of the MaVaN model

By minimizing the total thermodynamic potential, Eq. (13), and solving the mass equation, Eq. (16), numerically, we found the values of the scale factor and the sum of the neutrino masses at the critical point depending on the value of the model parameter  $\alpha$ , see Table 2. With an increase in the value of the model parameter  $\alpha$ , the value of the scale factor at the critical point decreases, *i.e.*, the moment of neutrino non-relativization occurs earlier, and as a consequence of this, the temperature at the critical point  $T_{cr}$  increases.

**TABLE 2** The values of the scale factor at the critical point,  $a_{cr}$ , the temperature at the critical point  $T_{cr}$ , the sum of neutrino masses at the critical point,  $m_\nu(a_{cr})$ , the sum of neutrino masses in the present epoch,  $m_\nu(a_0)$  in depending on the value of the model parameter  $\alpha$ .

$\alpha$	$a_{cr}$	$T_{cr}$	$m_\nu(a_{cr}) \text{ eV}$	$m_\nu(a_0) \text{ eV}$
0.0001	0.69	0.00034	0.0009	0.0021
0.0010	0.39	0.00061	0.0015	0.0109
0.0100	0.22	0.00109	0.0027	0.0507
0.0160	0.19	0.00120	0.0031	0.0700
0.1000	0.11	0.00223	0.0058	0.3020
0.1400	0.09	0.00260	0.0069	0.4365
0.1430	0.09	0.00260	0.0069	0.4473
0.3000	0.06	0.00416	0.0116	1.3179
0.5000	0.04	0.00668	0.0200	4.0291

<sup>4</sup>Neutrino masses  $m_\nu$  values are expressed in eV units

The dependence of values of the mass equation on the different values of the model parameter  $\alpha$  is presented in Fig. 2 . The value of the mass equation  $I_\alpha$  increases with an increase in the value of the model parameter  $\alpha$  and vice versa.

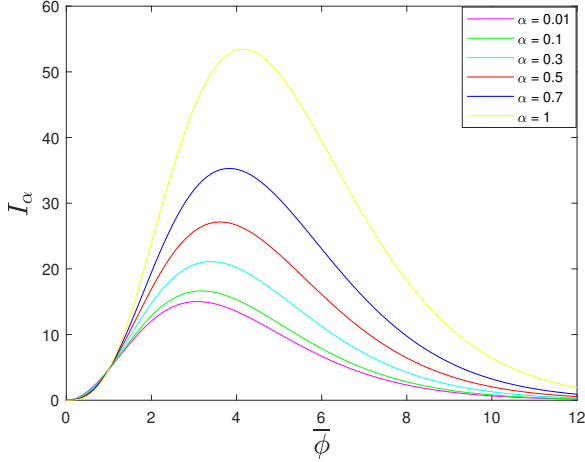


**FIGURE 2** The mass equation  $I_\alpha$ , under the assumption  $N_F = 3$ , for different values of the model parameter  $\alpha$ .

To study the evolution of neutrinos-scalar field fluid, we jointly numerically integrated the first Friedmann equation, Eq. (18), and the scalar field equation of motion, Eq. (19). We perform calculations for the flat MaVaN model, taking into account  $\Omega_{k0} = 0$  in Eq. (18). We studied how the value of the sum of neutrino masses depends on the value of the model parameter  $\alpha$ . With an increase in the value of the model parameter  $\alpha$ , the value of the initial sum of neutrino masses and, accordingly, the value of the sum of neutrino masses increases for all scale factors up to the present epoch, see Table 2 and Fig. 3 .

We investigated the influence of the neutrinos - scalar field fluid on the expansion rate of the universe. The expansion of the universe occurs more slowly with an increasing value of the parameter  $\alpha$  and vice versa for all values of the scalar factor, but only in the present epoch the expansion of the universe occurs equally regardless of the value of the model parameter  $\alpha$ , see Fig. 4 . In contrast to this fact, in the case of the scalar field with the Ratra-Peebles potential that does not interact with neutrinos, with an increase in the value of the parameter  $\alpha$ , the scalar field strengthens and, as a consequence, the expansion of the universe occurs faster Avsajanishvili, Arkhipova, Samushia, and Kahniasvili (2014). In the case of interaction of a scalar field with neutrinos and the formation of the neutrinos-scalar field fluid, with an increase in the value of the parameter  $\alpha$ , the sum of the neutrino

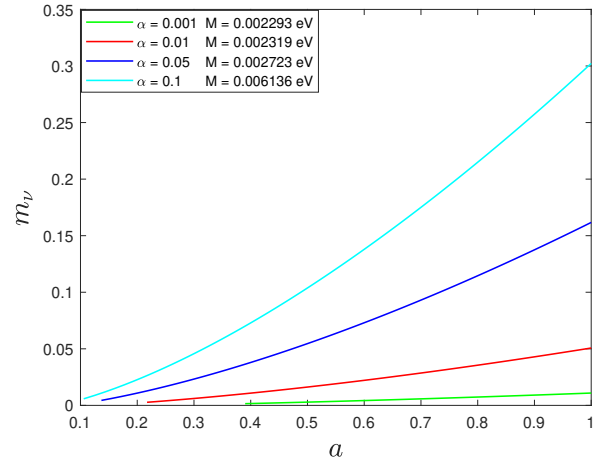


**FIGURE 3** The sum of neutrino masses (for  $N_F = 3$ ) for different values of the model parameter  $\alpha$  of the Ratra-Peebles potential.

masses (see Table 2 , Figs. (2 -3 )) increases and, accordingly, the scalar field weakens, which leads to a slowdown in the expansion of the universe.

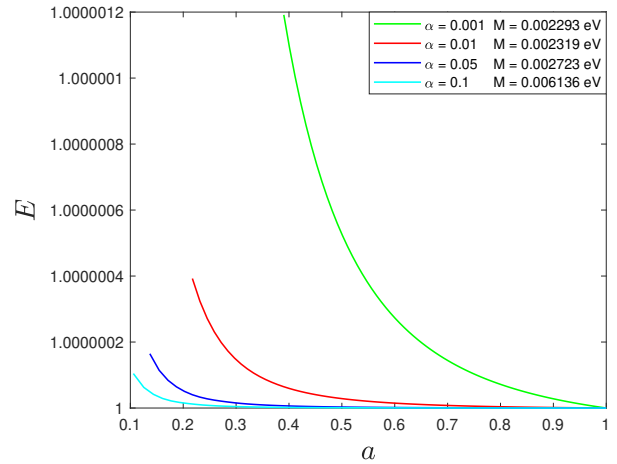


**FIGURE 4** Normalized expansion rate of the Universe in the MaVaN model taking into account  $N_f = 3$  for different values of the model parameter  $\alpha$ .

By studying the mutual influence of the value of the sum of neutrino masses and the value of the scalar field potential, we found that with an increase in the value of the model parameter  $\alpha$ , the value of the Ratra-Peebles scalar field potential also increases, see Fig. 5 . This happens because the scalar field

potential is defined in a certain range of neutrino masses, which depends on the value of the model parameter  $\alpha$ .

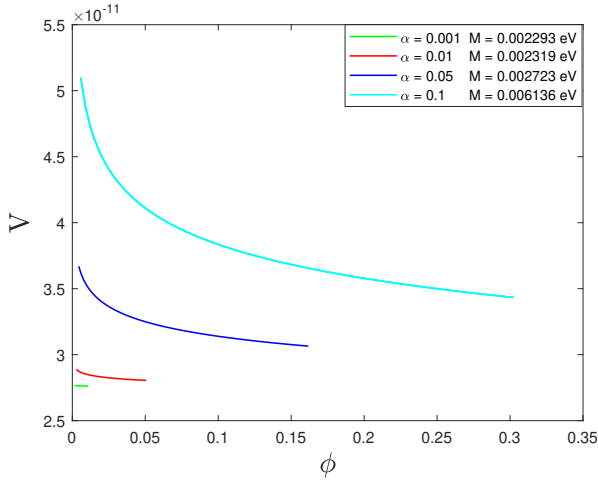


**FIGURE 5** The mutual influence of the sum of neutrino masses and the scalar field Ratra-Peebles potential for different values of the model parameter  $\alpha$ .

We explored the evolution of the mass of the scalar field with the Ratra-Peebles potential from the critical point  $a_{cr}$  to the present epoch  $a_0$  depending on the model parameter  $\alpha$ . With an increasing value of the model parameter  $\alpha$ , the mass of the scalar field decreases, while all these tracks converge to a zero mass value in the present epoch, see Fig. 6 .

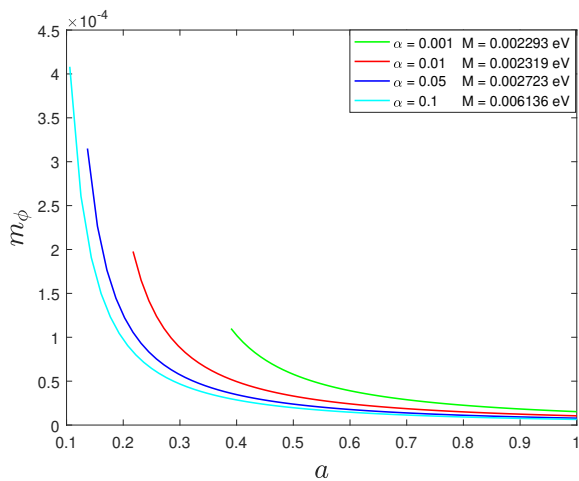


**FIGURE 6** The dependence of the mass of the scalar field with the Ratra-Peebles potential on the model parameter  $\alpha$ .

We studied the dependence of the total density of the thermodynamic potential of the neutrinos-scalar field fluid Eq. (14) at the critical point  $a_{cr}$  on different values of the model parameter  $\alpha$  at the fixed critical temperature  $T_{cr}$ . The results of these calculations are shown in Fig. 7 .

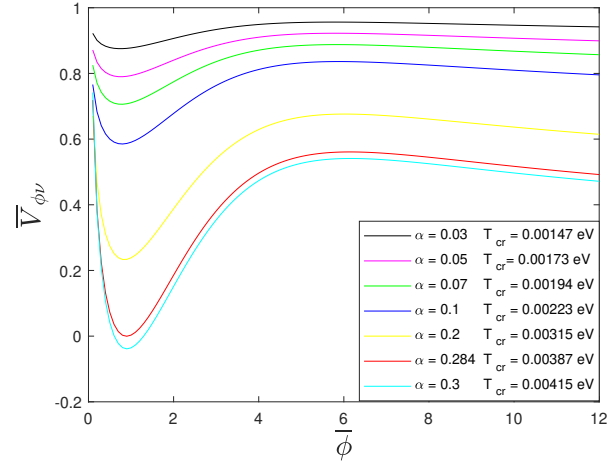


**FIGURE 7** The total density of the thermodynamic potential of the neutrinos-scalar field fluid (under the assumption  $N_F = 3$ ) at the critical point  $a_{cr}$  for different values of the model parameter  $\alpha$ .

With an increase in the value of the parameter  $\alpha$ , the temperature value at the critical point  $a_{cr}$  increases, the negative contribution to the density of the total thermodynamic potential of the fermionic field increases faster than the contribution of the scalar field, Eq. (14), which leads to a decrease in the value of the density of the total thermodynamic potential. In Fig. 7 can be identified: (i) the area of the minimum potential, or the area of the neutrinos oscillation, as well as (ii) the area of an unstable maximum, after which the density of the total thermodynamic potential rolls down to its minimum. Thus, the universe undergoes a phase transition from the (meta)stable oscillatory regime to the unstable rolling regime of the scalar field, which ultimately leads to the accelerated expansion of the universe.

## 5.2 | Carrying out observational constraints of the MaVaN model

The best-fit Hubble parameter values  $H(z)$  with  $1\sigma$ ,  $2\sigma$  and  $3\sigma$  confidence level including  $1\sigma$  error bars for the independent and correlated  $H(z)$  data to the flat and non-flat MaVaN models are presented in Fig. 8 (left panel) and Fig. 8 (right panel), respectively. Almost all of this data, at least for the most

part, cover the  $3\sigma$  range of the best-fit  $H(z)$  values for both flat and non-flat MaVaN models.

We obtained one-dimensional likelihoods and  $1\sigma$ ,  $2\sigma$ , and  $3\sigma$  confidence level contour constraints from the 32  $H(z)$  measurements on the parameters of the flat MaVaN model, Fig. 9 (left panel) and of the non-flat MaVaN model, Fig. 9 (right panel).

The best-fit parameter values and  $1\sigma$  and  $2\sigma$  confidence intervals for the flat and not-flat MaVaN models are presented in Table 3 and Table 4, respectively<sup>5</sup>. The observational  $H(z)$  data are consistent with the higher best-fit parameter values  $\mathbf{p} = \{H_0, \alpha, \Omega_{m0}, m_\nu\}$  for the non-flat MaVaN model compared to those for the flat MaVaN model.

**TABLE 3** The best-fit parameter values with confidence intervals of  $1\sigma$  and  $2\sigma$  for the flat MaVaN model.

Parameter	Best fit	$1\sigma$ interval	$2\sigma$ interval
$H_0$	64.04	[60.35, 65.52]	[59.77, 70.12]
$\alpha$	0.008	[0.002, 0.010]	[0.001, 0.016]
$\Omega_{m0}$	0.341	[0.292, 0.397]	[0.239, 0.438]
$m_\nu$	0.269	[0.038, 0.396]	[0.004, 0.567]

**TABLE 4** The best-fit parameter values with confidence intervals of  $1\sigma$  and  $2\sigma$  for the non-flat MaVaN model.

Parameter	Best fit	$1\sigma$ interval	$2\sigma$ interval
$H_0$	67.72	[61.25, 71.21]	[59.95, 77.55]
$\alpha$	0.010	[0.001, 0.014]	[0.000, 0.023]
$\Omega_{m0}$	0.396	[0.350, 0.475]	[0.269, 0.503]
$m_\nu$	0.273	[0.049, 0.473]	[0.010, 0.569]
$\Omega_{k0}$	-0.214	[-0.400, -0.037]	[-0.542, 0.129]

## 6 | CONCLUSION

Studying the interaction of the fermionic field (assuming that a number of neutrinos flavors  $N_F = 3$ ) and the scalar field with the Ratra-Peebles potential, we found that with an increase in the value of the model parameter  $\alpha$ : (i) the value of the mass equation  $I_\alpha$  increases; (ii) the moment of the neutrinos non-relativization occurs earlier; (iii) the temperature at the critical point increases; (iv) the value of the initial sum of neutrino masses and, accordingly, the value of the sum of neutrino

masses increases for all scale factors up to the present epoch; (v) the expansion of the universe occurs slower for all values of the scalar factor, but only in the present epoch the expansion of the universe occurs equally regardless of the value of the model parameter  $\alpha$ ; (vi) the value of the total density of the thermodynamic potential decreases, (vii) the mass of the scalar field decreases, while all these tracks converge to a zero mass value in the present epoch.

We carried out the observational constraints of the parameters for the flat and non-flat MaVaN models from 32  $H(z)$  data using the MCMC analysis. We found that almost all independent and correlated  $H(z)$  data, including  $1\sigma$  uncertainty, at least for the most part, cover the  $3\sigma$  range of the best-fit  $H(z)$  values for both flat and non-flat MaVaN models, see Fig. 8.

The observational data  $H(z)$  are consistent with the higher best fit parameter values  $\mathbf{p} = \{H_0, \alpha, \Omega_{m0}, m_\nu\}$  in the non-flat MaVaN model compared to those of the flat MaVaN model, see Tables (3 -4) and Fig. 9.

We obtained the following best-fit parameters for the flat MaVaN model: Hubble constant  $H_0 = 64.04^{+1.48}_{-3.69}$  km s<sup>-1</sup>Mpc<sup>-1</sup>, the model parameter of the scalar field Ratra-Peebles potential  $\alpha = 0.008^{+0.003}_{-0.006}$ , the matter density parameter in the present epoch  $\Omega_{m0} = 0.341^{+0.056}_{-0.050}$ , the sum of neutrino masses  $m_\nu \leq 0.396$  eV ( $1\sigma$  confidence level); while for the non-flat MaVaN model:  $H_0 = 67.72^{+3.50}_{-6.47}$  km s<sup>-1</sup>Mpc<sup>-1</sup>,  $\alpha = 0.01^{+0.004}_{-0.009}$ ,  $\Omega_{m0} = 0.396^{+0.079}_{-0.046}$ ,  $m_\nu \leq 0.473$  eV ( $1\sigma$  confidence level), the curvature density parameter in the present epoch  $\Omega_{k0} = -0.214^{+0.176}_{-0.187}$ .

Based on the results obtained, see Tables (3 -4), we can conclude that the MaVaN model, namely, the flat MaVaN model within the  $3\sigma$  confidence level and the non-flat MaVaN model within the  $2\sigma$  one, is capable of resolving the  $H_0$  tension.

## ACKNOWLEDGMENTS

This work was supported by **Shota Rustaveli National Science Foundation of Georgia (SRNSFG)** grant YS-22-998. The author thanks Bharat Ratra, Lado Samushia, Giorgi Khomeriki, Zack Brown, and Nick Magnelli for their hospitality in the Department of Physics, Kansas State University.

## Financial disclosure

This work was supported by **Shota Rustaveli National Science Foundation of Georgia (SRNSFG)** grant YS-22-998.

<sup>5</sup>Hubble parameter  $H_0$  values are expressed in km s<sup>-1</sup>Mpc<sup>-1</sup> units.



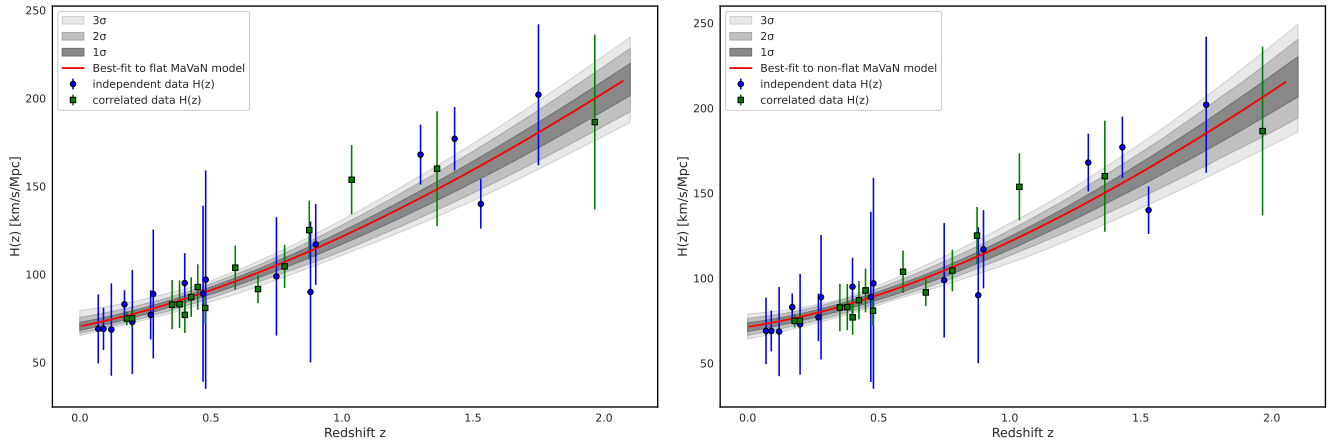


**FIGURE 8** Best-fit Hubble parameter values  $H(z)$  with  $1\sigma$ ,  $2\sigma$  and  $3\sigma$  confidence levels including  $1\sigma$  error bars for the independent and correlated  $H(z)$  data to the MaVaN model in the flat space (left panel) and in the non-flat space (right panel).

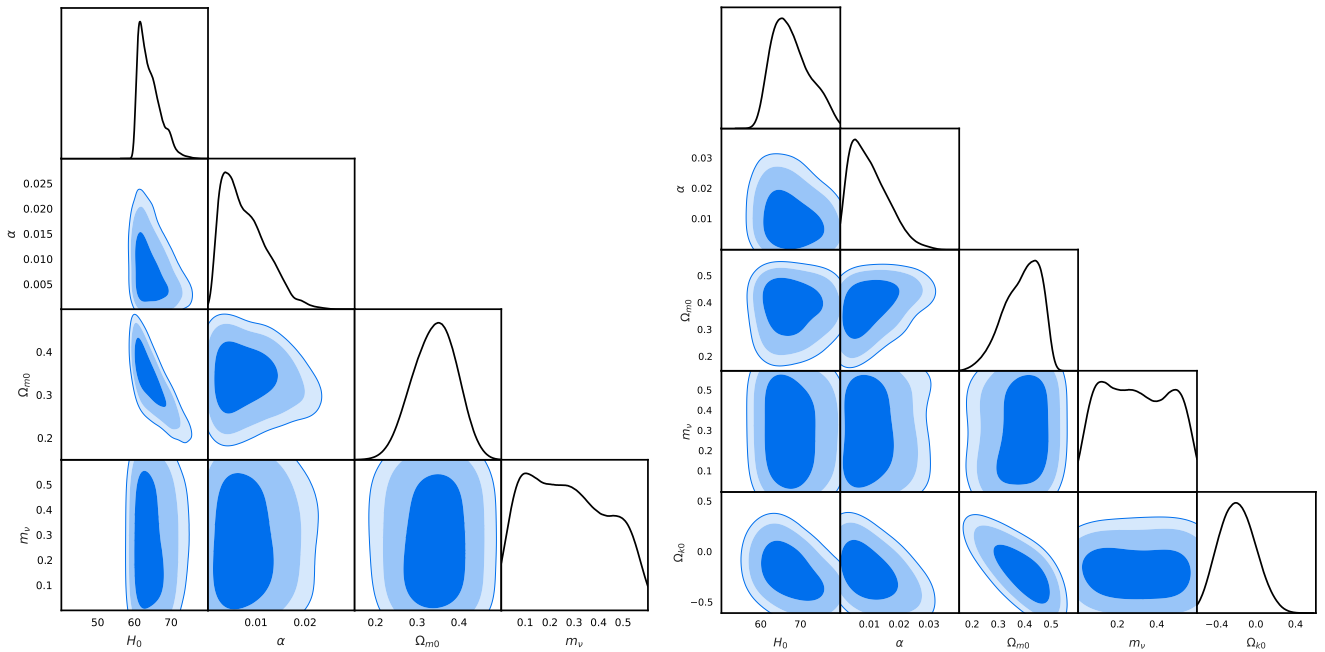


**FIGURE 9** One-dimensional likelihoods and  $1\sigma$ ,  $2\sigma$  and  $3\sigma$  confidence level contours constraints on the parameters of the MaVaN model from the  $H(z)$  measurements: for the flat space (left panel) and for the non-flat space (right panel).

## Conflict of interest

The author declares that there are no potential conflicts of interest.

## REFERENCES

Abdalla, E., & et al. (2022), *JHEAp*, 34, 49–211.  
 Abdul Karim, M., & et al. (2025, 3), *arXiv:2503.14738*.  
 Adame, A. G., & et al. (2024, 11), *arXiv:2411.12022*.

Adame, A. G., & et al. (2025), *JCAP*, 02, 021.  
 Afshordi, N., Zaldarriaga, M., & Kohri, K. (2005), *Phys. Rev. D*, 72, 065024.  
 Aghanim, N., & et al. (2020a), *Astron. Astrophys.*, 641, A1.  
 Aghanim, N., & et al. (2020b), *Astron. Astrophys.*, 641, A6.  
 Aiola, S., & et al. (2020), *JCAP*, 12, 047.  
 Aker, M., & et al. (2025), *Science*, 388(6743), adq9592.  
 Alam, S., & et al. (2021), *Phys. Rev. D*, 103(8), 083533.  
 Avsajanishvili, O., Arkhipova, N. A., Samushia, L., & Kahnishvili, T. (2014), *Eur. Phys. J.*, C74(11), 3127.  
 Ayaita, Y., Weber, M., & Wetterich, C. (2013), *Phys. Rev.*, D87(4), 043519.

- Bean, R., Flanagan, E. E., & Trodden, M. (2008a), *Phys. Rev. D*, **78**, 023009.
- Bean, R., Flanagan, E. E., & Trodden, M. (2008b), *New J. Phys.*, **10**, 033006.
- Berger, M. S., & Shojaei, H. (2006), *Phys. Rev. D*, **73**, 083528.
- Bjaelde, O. E., Brookfield, A. W., van de Bruck, C., Hannestad, S., Mota, D. F., Schrempp, L., & Tocchini-Valentini, D. (2008), *JCAP*, **01**, 026.
- Brookfield, A. W., van de Bruck, C., Mota, D. F., & Tocchini-Valentini, D. (2006a), *Phys. Rev. D*, **73**, 083515.
- Brookfield, A. W., van de Bruck, C., Mota, D. F., & Tocchini-Valentini, D. (2006b, Feb), *Phys. Rev. Lett.*, **96**, 061301.
- Brouzakis, N., Pettorino, V., Tetradis, N., & Wetterich, C. (2011), *JCAP*, **1103**, 049.
- Cai, R.-G., & Wang, A. (2005), *JCAP*, **03**, 002.
- Caldwell, R. R., & Kamionkowski, M. (2009), *Ann. Rev. Nucl. Part. Sci.*, **59**, 397-429.
- Cao, S., & Ratra, B. (2023), *Phys. Rev. D*, **107**(10), 103521.
- Casas, S., Pettorino, V., & Wetterich, C. (2016), *Phys. Rev.*, **D94**(10), 103518.
- Chitov, G. Y., August, T., Natarajan, A., & Kahnishvili, T. (2011), *Phys. Rev. D*, **83**, 045033.
- Collodel, L. G., & Kremer, G. M. (2012), *Grav. Cosmol.*, **18**, 196-200.
- Comelli, D., Pietroni, M., & Riotto, A. (2003), *Phys. Lett. B*, **571**, 115-120.
- del Campo, S., Herrera, R., & Pavon, D. (2008), *Phys. Rev. D*, **78**, 021302.
- del Campo, S., Herrera, R., & Pavon, D. (2009), *JCAP*, **01**, 020.
- Di Valentino, E. (2022), *Universe*, **8**(8), 399.
- Di Valentino, E., Mena, O., Pan, S. et al. (2021), *Class. Quant. Grav.*, **38**(15), 153001.
- Dolgov, A. D. (2008), *Phys. Atom. Nucl.*, **71**, 2152-2164.
- Elbers, W., & et al. (2025, 3), *arXiv:2503.1474*.
- Fardon, R., Nelson, A. E., & Weiner, N. (2004), *JCAP*, **10**, 005.
- Farrar, G. R., & Peebles, P. J. E. (2004), *Astrophys. J.*, **604**, 1-11.
- Gelman, A., & Rubin, D. B. (1992), *Statistical Science*, **7**(4), 457-472.
- Goh, L. W. K., Ocampo, I., Nesseris, S., & Pettorino, V. (2024), *Astron. Astrophys.*, **692**, A101.
- Hannestad, S. (2004), *New J. Phys.*, **6**, 108.
- Hu, J.-P., & Wang, F.-Y. (2023), *Universe*, **9**(2), 94.
- Huey, G., & Wandelt, B. D. (2006), *Phys. Rev. D*, **74**, 023519.
- Ichiki, K., & Keum, Y.-Y. (2008), *JCAP*, **06**, 005.
- Ivanchik, A. V., Kurichin, O. A., & Yurchenko, V. Y. (2024), *Universe*, **10**(4), 169.
- Jiang, J.-Q., Giarè, W., Gariazzo, S. et al. (2025), *JCAP*, **01**, 153.
- Kaplinghat, M., & Rajaraman, A. (2007), *Phys. Rev.*, **D75**.
- Kapusta, J. I., & Gale, C. 2011, *Finite-temperature field theory: Principles and applications*. Cambridge University Press.
- Kawasaki, M., Murayama, H., & Yanagida, T. (1992, January), *Modern Physics Letters A*, **7**(7), 563-570.
- Khalife, A. R., Zanjani, M. B., Galli, S., Günther, S., Lesgourgues, J., & Benabed, K. (2024), *JCAP*, **04**, 059.
- Lewis, A. (2019), *arXiv:1910.13970*.
- Lopez-Corredoira, M. (2023), *arXiv:2307.10606*.
- Madhavacheril, M. S., & et al. (2024), *Astrophys. J.*, **962**(2), 113.
- Mandal, S., Chitov, G. Y., Avsajanishvili, O., Singha, B., & Kahnishvili, T. (2021), *JCAP*, **05**, 018.
- Mandal, S., & Sehgal, N. (2023), *Phys. Rev. D*, **107**(12), 123003.
- Moresco, M. (2015), *Mon. Not. Roy. Astron. Soc.*, **450**(1), L16-L20.
- Moresco, M., Cimatti, A., Jimenez, R. et al. (2012, August), *J. Cosmology Astropart. Phys.*, **2012**(8), 006.
- Moresco, M., & et al. (2022), *Living Rev. Rel.*, **25**(1), 6.
- Moresco, M., Pozzetti, L., Cimatti, A. et al. (2016), *JCAP*, **05**, 014.
- Mota, D. F., Pettorino, V., Robbers, G., & Wetterich, C. (2008), *Phys. Lett.*, **B663**, 160-164.
- Naredo-Tuero, D., Escudero, M., Fernández-Martínez, E., Marcano, X., & Poulin, V. (2024), *Phys. Rev. D*, **110**(12), 123537.
- Nunes, N. J., Schrempp, L., & Wetterich, C. (2011), *Phys. Rev.*, **D83**, 083523.
- Palanque-Delabrouille, N., Yèche, C., Schöneberg, N., Lesgourgues, J., Walther, M., Chabanier, S., & Armengaud, E. (2020), *JCAP*, **04**, 038.
- Pavon, D., & Zimdahl, W. (2005), *Phys. Lett. B*, **628**, 206-210.
- Peebles, P. J. E. (1984), *ApJ*, **284**, 439-444.
- Peebles, P. J. E. (2022), *Annals Phys.*, **447**, 169159.
- Peebles, P. J. E., & Ratra, B. (2003), *Rev. Mod. Phys.*, **75**, 559-606.
- Perivolaropoulos, L., & Skara, F. (2022), *New Astron. Rev.*, **95**, 101659.
- Pettorino, V., & Baccigalupi, C. (2008), *Phys. Rev.*, **D77**.
- Pettorino, V., Wintergerst, N., Amendola, L., & Wetterich, C. (2010), *Phys. Rev.*, **D82**, 123001.
- Ratra, B., & Peebles, P. J. E. (1988a), *Phys. Rev.*, **D37**, 3406.
- Ratra, B., & Peebles, P. J. E. (1988b), *Astrophys. J.*, **325**, L17-L20.
- Riess, A. G., Breuval, L., Yuan, W. et al. (2022), *Astrophys. J.*, **938**(1), 36.
- Silvestri, A., & Trodden, M. (2009), *Rept. Prog. Phys.*, **72**, 096901.
- Tanabashi, M., & et al. (2018), *Phys. Rev.*, **D98**(3), 030001.
- Torrado, J., & Lewis, A. (2021), *JCAP*, **05**, 057.
- Tristram, M., & et al. (2024), *Astron. Astrophys.*, **682**, A37.
- Vagnozzi, S. (2023), *Universe*, **9**(9), 393.
- Velten, H. E. S., vom Martens, R. F., & Zimdahl, W. (2014, nov), *Eur. Phys. J.*, **C74**(11), 3160.
- Wetterich, C. (1988), *Nucl. Phys.*, **B302**, 645-667.
- Wetterich, C. (2007), *Phys. Lett.*, **B655**, 201-208.